Europium doped titanium dioxide nanocrystalline: synthesis, structure and optical properties

I. A. S. Adriss[b, c], F. Shaban[b], M. Y. A. Yagoub[e,d], H. Wardi[a], Nashwa A. Issa[b] and Hassan H. Abuelhassan[b]
[a] Physics Department, Omdurman Alahlia University, Omdurman, Sudan.
[b] Department of physics, Al Neelain University, PO Box 12702, Khartoum, Sudan.
[c] Department of physics, University of Zalingei, Central Darfur, Sudan.
[e] Department of Physics, Sudan University of Science and Technology, PO Box 407, Khartoum, Sudan.
[d] Department of Physics, University of the Free State, PO Box 339, Bloemfontein, ZA9300, South Africa.
[*]Corresponding author: hssnwardi0@gmail.com, Fatima.shabaan@gmail.com (H.Wardi)

DOI: https://doi.org/10.56807/buj.v5i1.361

Abstract

Uniform, spherical-shaped TiO_2: Eu nanoparticles with different doping concentrations were synthesized using the sol-gel method. The structural, morphology, optical, luminescent, and surface properties of the samples were investigated at different Eu^{3+} concentration. The morphology, crystalline structure, and chemical composition of the samples were characterized by scanning electron microscopy, X-ray diffraction, and X-ray photoelectron spectroscopy. The X-ray diffraction results reveal that the obtained powder nanoparticles consist of a single phase tetragonal structure. The crystallite sizes calculated by utilizing Scherrer's equation were found in the range of 18.94 – 7.77 nm for TiO_2:Eu samples annealed at 550^{o}C. The SEM images reveal an irregular agglomerated morphology indicating a decrease in particle size with an increase in Eu3+ concentration. X-ray photoelectron spectroscopy (XPS) high resolution spectra of the Ti-2p peak confirmed that Ti atoms were in a doubly ionized state, and the deconvolution of the O1s XPS peak show the presence of oxygen related defects in the sample. EDS results confirm a systematic increase of Eu content in the as-prepared samples with the increase of europium concentration. Incorporation of europium in the titania particles induces a structural deformation and a blueshift of their absorption edge. The luminescence intensity increases with Eu^{3+} concentration up to 3 mol% and then quenched. While the PL emission of the as-grown samples is dominated by the $^5D_0$ - ^7F_j transition of Eu^{3+} ions, the emission intensity reduces drastically after thermal annealing due to outwards segregation of dopant ions.

Keywords: *Titanium dioxide; Photoluminescence Spectroscopy; XPS; Nanocrystalline; Anatase; Rutile.*

1.Introduction

Synthesis of semiconductor nanoparticles with modified properties has attracted and gained important scientific interest in the field of nanoscaled sciences. The interest in these nanomaterials is aggravated by the exclusive optical, electrical and photoluminescent properties induced by the quantum size effect which made them talented materials for various potential applications (Tiwana, Docampo, Johnston, Snaith, & Herz, 2011), (Leostean, et al., 2013). TiO_2 is an outstanding semiconducting material and is extensively used in numerous applications such as gas sensors, solar cells, protective coatings, biological activities and photocatalysts (Ogawa, et al., 2008), (Toma, et al., 2006). However, TiO_2 takes an amorphous form in preparation (at room temperature), and crystallizes at higher annealing temperatures. TiO_2 under calcination crystallizes to different forms of anatase, rutile and brookite (Reddy, Manorama, & Reddy, 2003). The brookite phase stabilizes at low temperatures, which makes it practically can be utilized in dye-sensitized solar cells (DSSC) (Jiang, Kitamura, Yin, Ito, & Yanagida, 2002). The structure of the brookite is orthorhombic, while the anatase and rutile phases are tetragonal with a difference in the phase groups. The anatase phase has space group $I4_1/amd$ (W. Li, Lin, Huang, & Shah, 2004) with four units of formula in a one-unit cell, while the rutile phase contains space group $P4_2/mnm$ with two TiO_2 formula units in one-unit cell (W. Li, Lin, Huang, & Shah, 2004), (Linsebigler, Lu, & Yates, 1995). Each crystalline phase has its physical properties, such as the band gap and surface states (Koelsch, Cassaignon, Guillemoles, & Jolivet, 2002), (Tang, Prasad, Sanjines, Schmid, & Levy, 1994). Doping with metal ions has been confirmed to be a probable route for the development of photoactivity of titanium dioxide and improved photoactivity has been observed by transition metal ion doping (Choi, Termin, & Hoffmann, 1994), (C, M, O, Suciu, R.C, & T.D., 2013). Rare-earth-metal compounds, chiefly their oxides, have become of increasing consideration in recent years because of their special photoluminescence and catalytic properties (T. Lo´ pez, 2001), (MASUDA & Akimasa, 2001). Lanthanide ions are known for their capability to form complexes with a variety of Lewis bases (e.g., acids, amines, aldehydes, alcohols, thiols, etc.) in the interaction of these functional groups with the f-orbitals of lanthanides (Sibu, Kumar, Mukundan, & Warrier, 2002), (Yuhong, Huaxing, X.Yongxi, & Yanguang, 2003). It is estimated that the incorporation of lanthanide ions into a TiO_2 matrix could supply a means to concentrate the organic pollutant at the semiconductor surface and therefore enhance the photoactivity of titania (Z, Q, & al., 2005). Eu–doped titanium dioxide (TiO_2:Eu) is a large band-gap semiconductor with many attractive properties. The long emission lifetime and rich spectral properties of Eu ions are highly attractive in various ways. Inertness to the chemical environment, long-term photostability, excellent electrical and thermal conductivity, corrosion resistance, and non-toxicity have made TiO_2 a significant component in many sensible applications and commercial products, such as electronics, optics, photocatalysis, biotechnologies, sensors and other material science fields (Pal, Pal, Jiménez, & Pérez-Rodríguez, 2012), (Javier Navas, 2014), (M. Stefan, 2013), (Dihingia & Rai, 2012). A variety of synthesis methods are used to prepare Eu doped TiO_2 nanoparticles such as thermal hydrolysis, sol-gel, hydrothermal processes and

microemulsion processes. Among these various methods, sol-gel is an attractive method because the sol-gel technique has many advantages over other preparation methods such as the capability of controlling the textural and surface properties and doping level, the simplicity and also, and the low-temperature processing. This helps in the process of controlling the different parameters of the materials, such as the surface area, average crystallize size, powder morphology and phase structure (R. Nainani, 52-58.), (Z. Sarteep, 2016). There are several studies performed to improve the nanoparticle properties by depositing noble metals and introducing surface modifiers and dopants (Sharmy Saimon Mano, 2012,), (B. Balasubramanian, 2010). The purpose of the present work is to study the effect of europium dopants on the composition and optical properties of TiO_2, by investigating their effect on the formation of the phase and also the change in the energy bandgap.

2. Experiment

TiO_2 doped with different Eu concentrations was prepared using the hydrolysis process. Titanium tetra chloride ($TiCl_4$), europium nitrate (111) with a purity of 99.9%, and Ammonium hydroxide (NH_4OH) were used as precursors. Reaction-grade ethanol (CH_3CH_2OH) with a purity of 99.9% and deionized water were used as solvents. The precursors were obtained from Sigma Aldrich and used without any further purifications. In the typical process, europium nitrate was dissolved in 50 ml of deionized water, 3.5 ml of titanium tetra chloride was added dropwise to the previous solution while it was being kept in an ice bath under a fume hood, then 35 ml of ethanol was added and the solution was vigorously stirred for 30 min at room temperature. Drops of ammonium hydroxide were added wisely into the solution to adjust the pH from 0 to 10. The stock solution was continuously and vigorously stirred until a white gel was formed. The gel was aged for 20 hours before any further process. Finally, the obtained gel was washed with deionized water using a centrifuge to remove chloride ions and all unwanted chemicals from the gel, and then they were dried at 120 $^{\circ}$C in air for five hours. This resulted in the formation of a white precipitate (powder). The precipitates were annealed in air at 550^{o}C for 5 h. The Eu concentration varied from 0.5 mol %, 1 mol %, 3 mol % and 5 mol %.

3. Characterization

The structural properties of the undoped TiO_2 and Eu:TiO_2 powders were analyzed using a Bruker D8 Advance powder diffractometer with a Cu Kα radiation of wavelength 0.154 nm. The scanning electron microscopy (SEM) of the powder was performed using a JEOL JSM-7800F microscope for analysis of the morphology. The diffuse reflectance (DR) spectra measurements were recorded using a Lambda 950 UV-vis spectrophotometer with spectralon integrating sphere accessory. For the PL measurements of the europium doped titanium dioxide powders a Cary Eclipse spectrophotometer was used at room temperature with a monochromatized xenon flash lamp as the excitation source. The cathodoluminescence (CL) emission spectra were measured using a Gatan MonoCL4 accessory fitted to the JEOL JSM-7800F system in a vacuum of the order of 10-5 - 10-6 Torr and electron energy of 5 keV. The Auger Electron Spectroscopy (AES) was used to study the chemical composition of the compounds. The powder was bombarded by an electron beam with a current density of ~ 1.27 mA/cm^{-2}, a beam current of ~ 3 µA and an acceleration voltage of ~2 kV. The Auger peak to peak heights (APPH) was collected

simultaneously using the same electron beam. The Energy Dispersive X-ray Spectrometer (EDS) and X-ray photoelectron spectroscopy (XPS) were used for the chemical composition analysis. XPS analysis was performed before and after degradation to evaluate the differences and changes in the surface chemical composition. MultiPak software was utilized to analyze the spectra to determine the chemical compounds and their electronic states using Gaussian–Lorentz fits.

4. Results and discussion

4.1 Structural analysis

The XRD patterns of the undoped and Eu-doped TiO_2 powder annealed at 550°C Figure 1 reveal the presence of TiO_2 exclusively in an anatase (tetragonal) phase (JCPDS 84-1286). In general, the intensity of the diffraction peaks decreases greatly with the increase of doping concentration, indicating a loss of crystallinity due to lattice distortion. When Eu^{3+} ions are incorporated into the periodic crystal lattice of TiO_2, a strain is induced into the system, resulting in the alteration of the lattice periodicity and a decrease in crystal symmetry. As can be seen from the XRD patterns, the diffraction peaks get broadened as the Eu^{3+} concentration is increased, suggestive of a systematic decrease in the grain size. The crystallite size of undoped and Eu doped TiO_2 samples was calculated by using Scherrer's equation (M. H. M. Abdelrehman, 2020).

$$D = K\lambda / \beta \cos\theta \qquad (1)$$

where D represents the crystallite size, λ is the X-ray wavelength (1.54056 Å), β is the full width at half maximum (FWHM) of the diffraction peak (in radians), K is constant-coefficient (0.89) and θ is the diffraction angle at the peak maximum (in radian).

To calculate the lattice parameters of the samples Bragg's law was used as follow:

$$d_{(hkl)} = \lambda / 2 \sin\theta \qquad (2)$$

d(*hkl*) is the interplanar spacing between the crystal planes (*hkl*); λ is the X-ray wavelength; θ is the diffraction angle. $d(hkl) = (h^2/a^2 + k^2/a^2 + l^2/c^2)^{-1/2}$.

The crystallite size and the lattice parameter of the samples were evaluated (Table 1). Here, *hkl* are the Miller indices; a, b, and c are the lattice parameters (in a tetragonal system, $a = b \neq c$). As can be seen from the estimated data, the estimated lattice parameters and unit cell volume values for the doped TiO_2 nanoparticles deviate considerably from those of the undoped sample due to the incorporation of Eu^{+3} ions into the TiO_2 lattice, which induces the local distortion of the crystal structure.

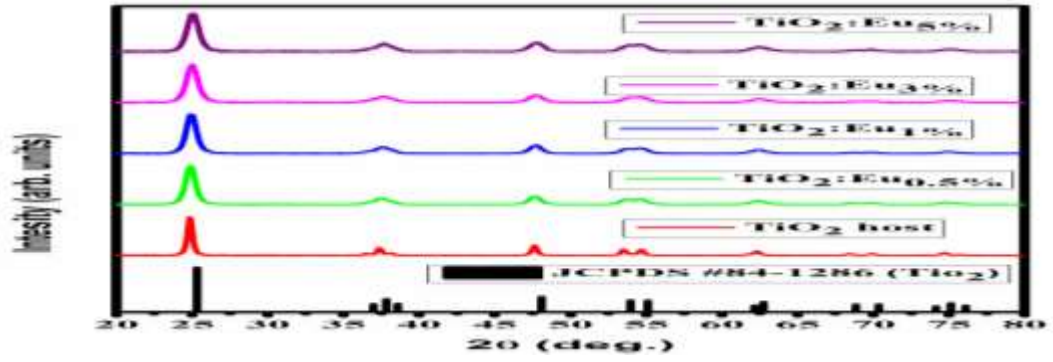

Figure 1: XRD patterns of the undoped and Eu doped TiO_2 different concentrations powders annealed at 550°C and standard.

Table 1: Crystallite size and lattice parameters of TiO_2 doped with various Eu concentrations annealed at 550 °C.

Eu concentration/ mol%	Crystallite size (nm)	Lattice parameters/(Å)	
		a= b	C
0.0	18.94	4.13	7.16
0.5	9.13	4.13	7.15
1.0	8.72	4.12	7.13
3.0	7.80	4.11	7.12
5.0	7.77	4.10	7.10

4.2 Surface morphology

The SEM images of undoped and Eu doped TiO_2 nanoparticles of different concentrations annealed at 550°C are presented in Figure 2. The formation of titania nanoparticles of a spherical morphology and narrow size distribution can be seen from the SEM micrographs. Compared with the undoped TiO_2 Figure 2(a), the average size of the Eu-doped TiO_2 nanoparticles Figure 2(b-e) decreases almost exponentially with the increase of the dopant concentration, suggesting that the incorporation of Eu ions suppresses the growth of TiO_2 nanocrystals to a great extent

.

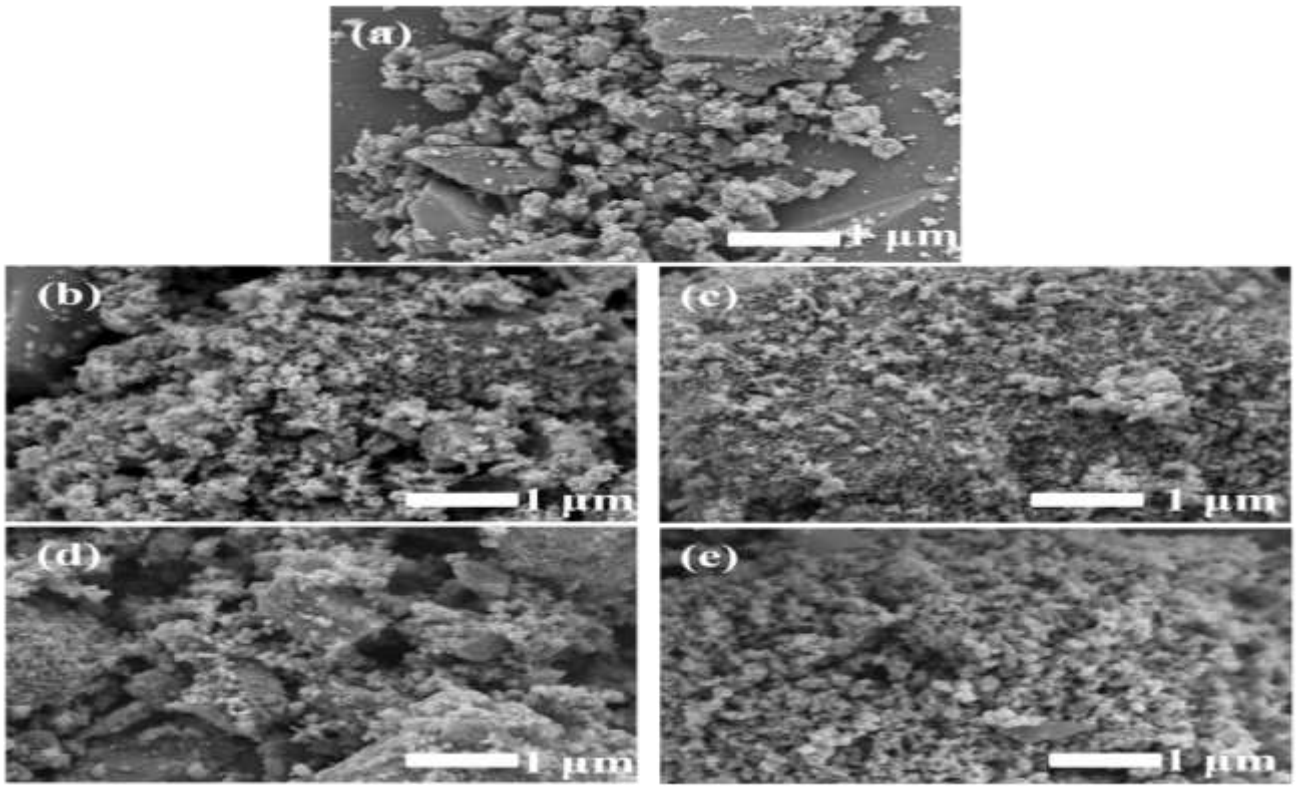

Figure 2: SEM images of (a) the undoped TiO_2 and TiO_2:Eu (b) 0.05, (c) 1, (d) 3 and (e) 3 mol%, annealed at 550°C.

4.3 Surface analysis

Figure 3 shows the AES of the undoped TiO_2 and Eu doped TiO_2 powder annealed for 5 h at 550ºC before and after degradation in an oxygen atmosphere. The Eu concentration, did not alter the AES peak' as in XRD position of the major diffraction peaks but caused a notice reduction in the peaks' intensity The Auger peaks of the principal elements were detected at 389 and 424 eV for Ti and 510 eV for O. In addition, C is also detected. The C is due to adventitious contamination of the surface during handling and exposure of the sample to the atmospheric environment. To verify the presence of Eu in the doped samples, they were analyzed by EDS. In the EDS spectra and estimated composition of the samples are presented in Figure 4. The EDS spectra reveal that the emission peaks correspond to O, Ti, and Eu, along with the carbon peak which might have come from the carbon tape used to fix the samples on the sample holder. A systematic decrease in the content of titanium and an increase in the relative content of europium are observed with the increasing nominal concentration of the dopant in the samples

.

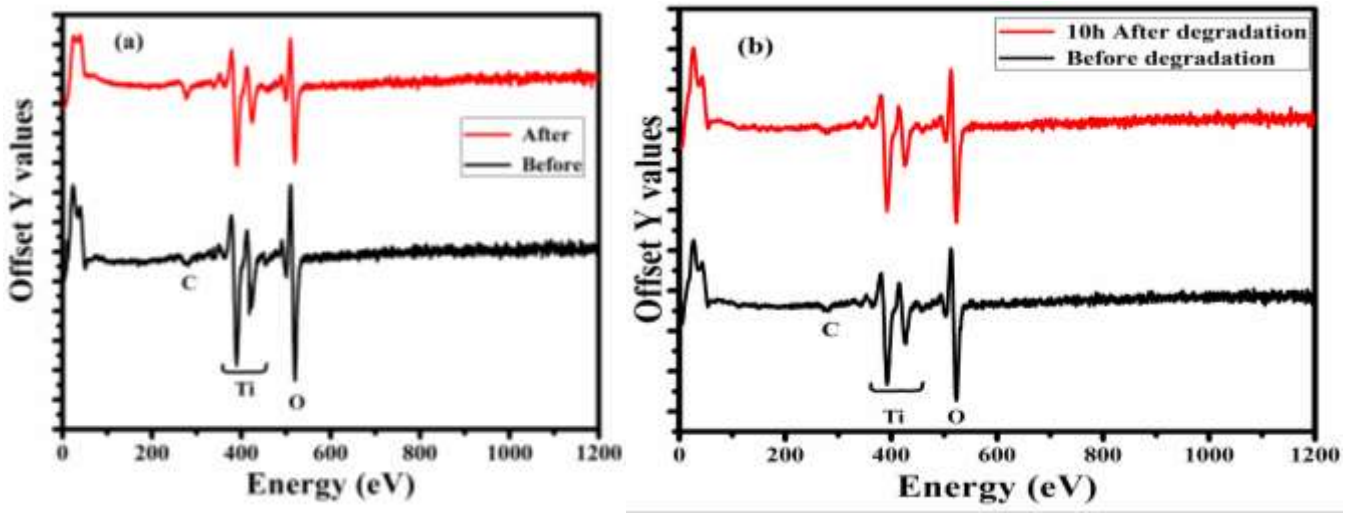

Figure 3: (a) AES of undoped TiO_2 and(b) AES of the TiO_2:Eu (5mol%) annealed at 550ºC.

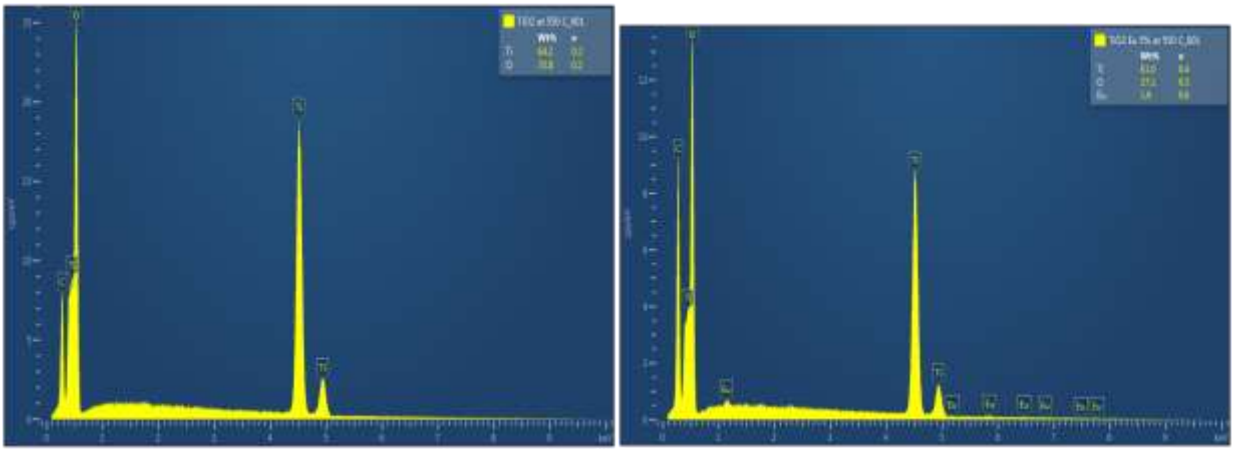

Figure 4: EDS of undoped $TiO_2$and TiO_2:Eu (5mol%) annealed at 550ºC.

4.4 Chemical analysis

Quantitative XPS analysis was performed on the europium (5mol%) doped titanium dioxide powder annealed for 5 h at 550ºC. Typical survey and high-resolution spectra of the second P orbital (Ti 2p) level of Eu^{3+} doped TiO_2 obtained in oxygen pressure (after 30s of Ar^+ ion sputtering) are presented in Figure. 5. The observed binding energies and full-widths-at-half-maximum (FWHM) are summarized in table 2. Two peaks attributed to the Ti 2p3/2 and Ti 2p1/2 lines were detected at binding energies of 458.48, 464.12, 458.91 and 464.52 eV, respectively. The peak separation of 5.64 and 5.61 eV between the Ti 2p1/2 and Ti 2p3/2 signals. These values comfortably match the standard reference value of Ti (Yuta Tanaka1, 2008). No metallic Ti could be detected, which is in agreement with the XRD measurements. According to the deconvolution results, the Ti 2p spectrum of the sample is dominated by species in the Ti^{4+} oxidation state with the presence of contribution of reduced species Ti^{3+} and Ti. The presence of lower oxidation states could be attributed to the reduction of the initial TiO_2 nanoparticles during laser processing. As a consequence, the composition of the sample will be different in the depth as compared to the top surface, which is fully oxidized due to air exposure. On the other hand, it was reported that Ar^+ sputtering can induce changes in the chemical states of transition metal oxides, stoichiometric oxides being reduced, resulting in additional components in the XPS spectra, However, the intensity of the lines was reported to increase gradually with the increase of the sputtering time during the first 15 min (Su, et al., 2013), in contrast to our results.

Deconvoluted oxygen in the ground state (O 1s) peaks for the TiO_2:Eu^{3+} powder obtained at oxygen pressure after sputtering, high oxygen pressure is shown in Figure5. The O 1s peak was de-convoluted by using the Gaussian-Lorentz function, and three components were found as marked as O1, O2 and O3. These components were always explained as follows: O1 is due to the O^{2-} ions in the Ti-O-Ti network of the wurtzite structure, O2 was ascribed to the O^{2-} in deficient regions such as oxygen related defects and hydroxyl group, and O3 is due to the chemisorbed species and loosely species on the surface. The O2 and O3 components decrease after the sputtering for the sample whereas O1 increases, which can be attributed to the removal of the surface contaminations (Stefanov, 012039), (Ketteler, 2007), (Simonsen, 2009) (Wang, 2013), (Leshuk, 2013), (Jribi, 2009). The details of the de-convoluted O 1s components are given in table 3.

Table 2: Binding energies and full-widths-at-half-maximum (fwhm) of TiO_2: Eu .

Sample	Peaks position (eV)	FWHM	% Gaus
Eu^{3+} 0 mol%	458.48	1.26	90
	464.12	2.00	60
	456.88	2.60	60
	460.44	2.50	70
	458.78	1.90	70
	462.48	1.50	90
Eu^{3+} 5 mol%	458.91	1.24	70
	464.52	2.09	60
	457.33	2.60	80

	460.44	1.94	70
	455.25	1.90	70
	462.65	1.82	90

Table 3: Peak position and area of the O1s de-convoluted components.

Sample	Peaks name	Peaks position (eV)	Area %
Eu^{3+} 0 mol%	O1	530.00	78
	O2	531.60	68
	O3	529.56	68
Eu^{3+} 5 mol%	O1	530.26	69
	O2	531.60	68
	O3	529.60	49

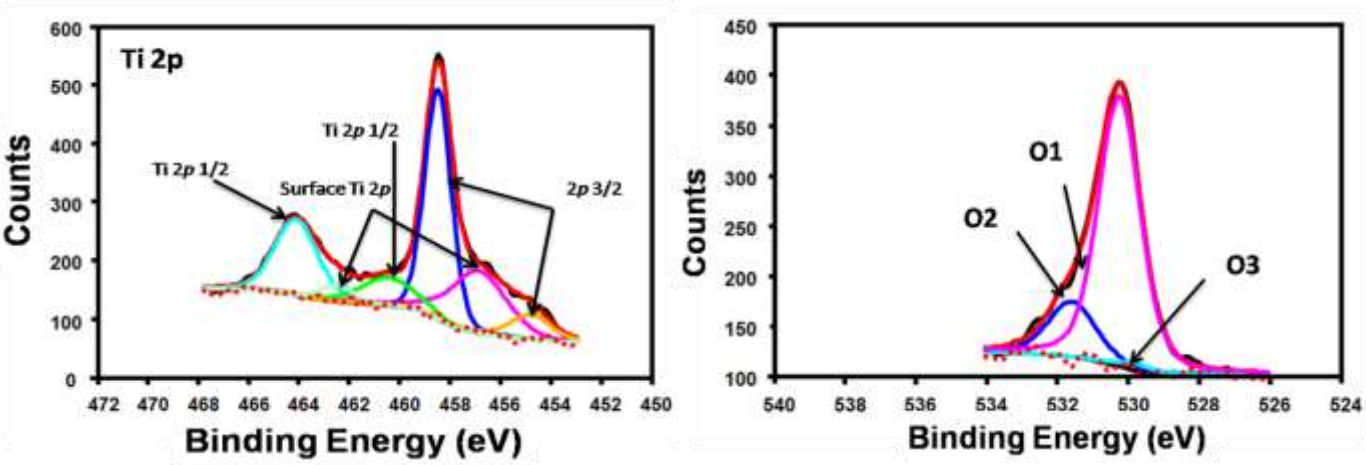

Figure 5: High-resolution XPS spectra of Ti 2p peaks and O 1s peaks.

4.5 Diffuse reflection spectra and band gap analysis

Spectroscopic measurement of diffuse reflectance in UV-Vis spectral range is a standard technique for the determination of the band gap of powder samples (Simmons, 1974). Figure 6 (a) shows the diffuse reflectance spectra of the undoped and Eu-doped titania powders annealed at 550ºC. A sharp decrease in reflectance started at about 371 nm for the undoped TiO_2 samples due to strong absorption. On increasing the incorporated Eu content, the absorption edge suffered a gradual blueshift. Figure 6(b) presents the Tauc plots for the undoped and Eu-doped samples used to determine their band gap energy associated with an indirect transition. The well-known Tauc law (Equations 3 and 4) (Sharma, 2012) was used to estimate the energy band gap of the samples:

$F(R_\infty) = (1 - R_\infty)^2 / 2R_\infty$ (3)

$\alpha h\nu = C(h\nu - Eg)^m$ (4)

where $F(R_\infty)$ was substituted by the absorption coefficient (α), $h\nu$ is the incident photon energy, C is a constant, Eg is the optical band gap energy and $m = 2$ for indirect band gap material. The calculated energy band gap of the undoped and Eu doped samples are tabulated in the table 4. It can be observed that the indirect band gap

increases gradually with the increase of doping concentration. However, the estimated indirect band gap values (3.27 to 3.36 eV) for all the samples were very close to the reported indirect band gap value of anatase (Asahi R, 2000). With the increase of incorporated Eu content, the band gap energy of the TiO_2 nanostructures increases systematically. This behavior is very similar to the previously reported results (Kumar S, 2011), where the authors observed a blueshift in the band gap of Eu-doped CdS nanorods with the increase of doping concentration. The reason for such band gap energy increment has been proposed as the gradual movement of the conduction band of TiO_2 above the first excited state of Eu^{+3} due to the increased dopant incorporation. Incorporated Eu^{+3} ions at the first excited state interact with the electrons of the conduction band of TiO_2, resulting in a higher energy transfer from the TiO_2 to Eu^{+3} ions. However, increased absorption in the visible range and redshift of the energy band gap have been observed by Yu et al. on doping TiO_2 nanotubes with Fe^{+3} ions. Such an opposite behavior has been explained through the creation of dopant levels near the valence band of TiO_2 on Fe^{+3} ion incorporation. Therefore, the relative shift of the absorption edge of the semiconductor depends strongly on the difference between the ionic radius of the dopant and the host cations, as well as on the chemical nature of the dopants (Yu J, 2009).

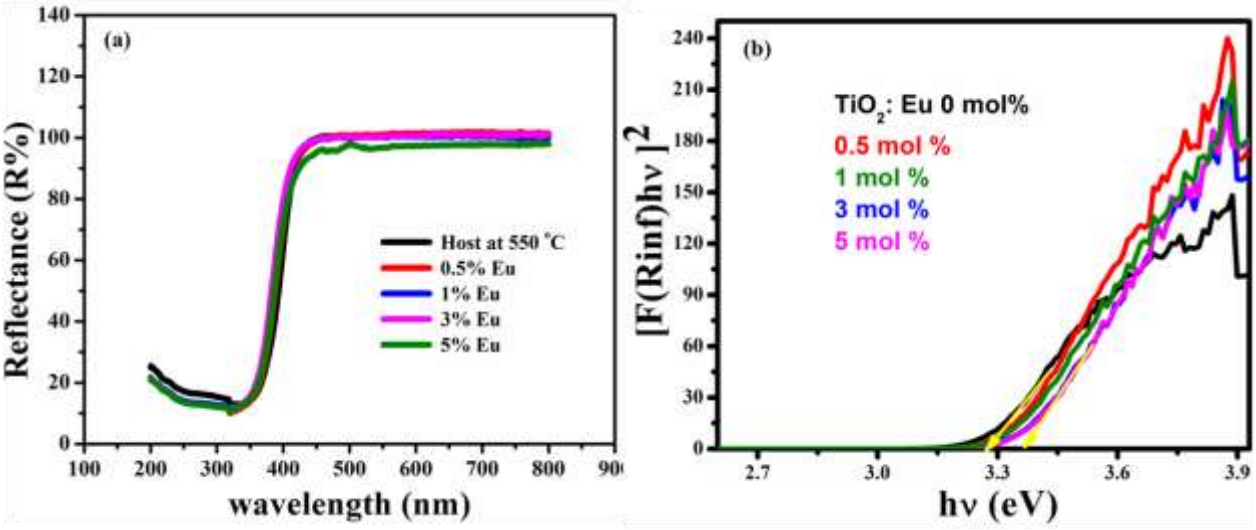

Figure 6: (a) Reflectance spectra of undoped and Eu:TiO_2 different concentrations annealed at 550ºC, (b)Tauc plots and band gap energy estimation of host and Eu: TiO_2 nanoparticles for indirect transition.

Table 4: Band gap of TiO_2 doped with various Eu concentrations annealed at 550 °C.

Eu concentration/ mol%	The band gap (eV) of samples annealed at 550 °C
0.0	3.27
0.5	3.33
1.0	3.35
3.0	3.36
5.0	3.36

4.6 Photoluminescence Spectroscopy (PL)

The excitation wavelength fixed at 465 nm the PL emission spectra were recorded for Eu^{3+} doped TiO_2 nanoparticles varying Eu^{3+} concentration (0.5, 1, 3 and 5 mol%) as shown in Figure 7(a). The emission intensity initially increases with increasing of the Eu^{3+} concentration up to 3mol% and then decreases due to concentration quenching phenomena, it is mainly caused by the nonradiative energy transfer among Eu^{3+} ions, which usually occurs as a result of an exchange interaction, radiation reabsorption, or a multipole–multipole interaction (S. Yao, 2011).

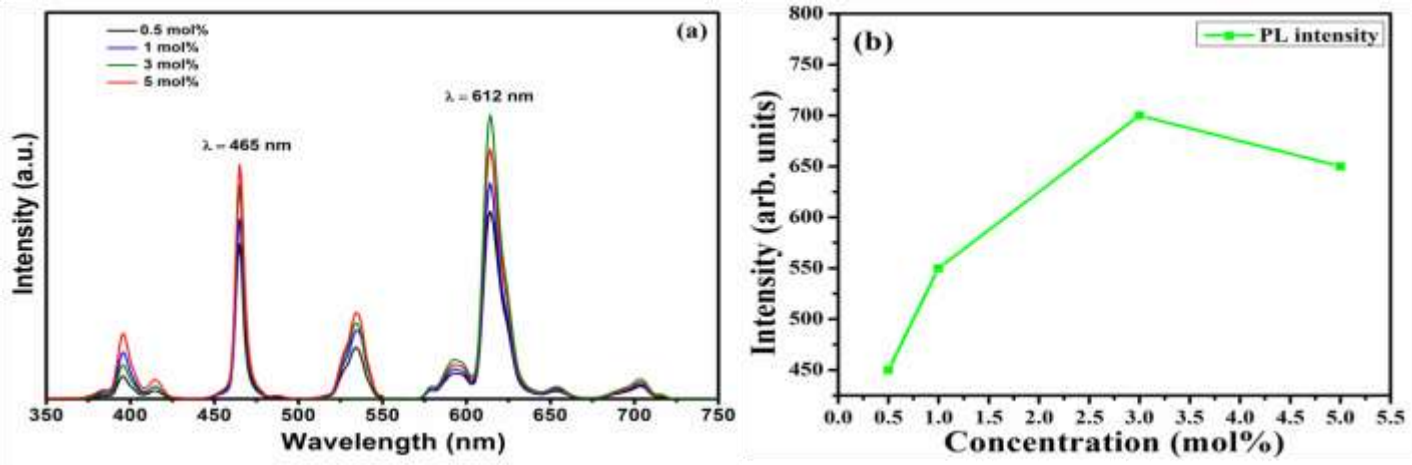

Figure 7: (a) PL spectra of TiO_2 doped with Eu different concentrations annealed at 550°C. (b) PL intensity as function of Eu^{3+} concentration.

The sample Eu^{3+} concentration of 3mol% was considered as an optimum sample, thereafter, the 3mol% was subjected to different annealing temperatures of 550°C, 700°C, 850°C and 1000°C to study the transition of this particular sample. Figure 8(a) shows the PL spectra of the optimum concentration of Eu doped titania nanoparticles annealed at different temperatures. Eu^{+3} doped titania nanoparticles show several sharp and well-resolved emission lines associated with Eu^{+3} ions which correspond to radiative relaxations from the $^5D_0$ level to its low lying multiplets ^7Fj (j = 0, 1, 2, 3), known as "intrafshell transitions" (McHale, 2012). The strongest emission centered at around 612 nm corresponds to the electrical dipole transition ($^5D_0$ - $^7F_2$) of Eu^{+3} ions which give the red color to the luminescence signals. In the literature, it has been reported that this transition is possible only if Eu^{+3} ions occupy a site without an inverse symmetry (Frindell KL, 2002). Other emission peaks centered around 570, 586 and 674 nm are associated with $^5D_0$ - $^7F_0$, $^5D_0$ - $^7F_1$ (magnetic dipole transition), $^5D_0$ - $^7F_3$ transitions of Eu^{+3} ions, respectively. All the above mentioned trasnsions are in agreement with the standard emission and excitation processes showed in Figure 8(b). With increasing in the annealed temperature the PL intensity decreases systematically as can be seen in figure 8(c). It's clear that the intensity behaves differently at annealing temperature of 700°C which is attributed to the fact that at 700°C the sample form mixed phases of anates and rutile. Commonly, PL emission of anatase TiO_2 is attributed to three different physical origins: self-trapped excitons, oxygen vacancies, and surface states (defect) (Lei Y, 2001). This visible

luminescence band arises from the radiative recombination of electrons via intrinsic surface states of TiO_2 nanoparticles (Liu Y, 1997). It is well known that in case of nanoparticles, surfaces play important roles as the surface-to-volume ratio becomes increasingly large at nanometer size. As TiO_2 is a strongly ionic metal oxide, the filled valance band is mainly composed of the outermost 2*p* orbitals of oxygen atoms, and the lowest conduction band is derived from titanium 3*d* orbitals. When some titanium atoms are exposed to the surface of nanoparticles, they get oxidized into Ti^{+3}, Ti^{+2}, or Ti^{+} oxidation states, and localized energy levels are introduced within the forbidden gap (Zhang WF, 2000).

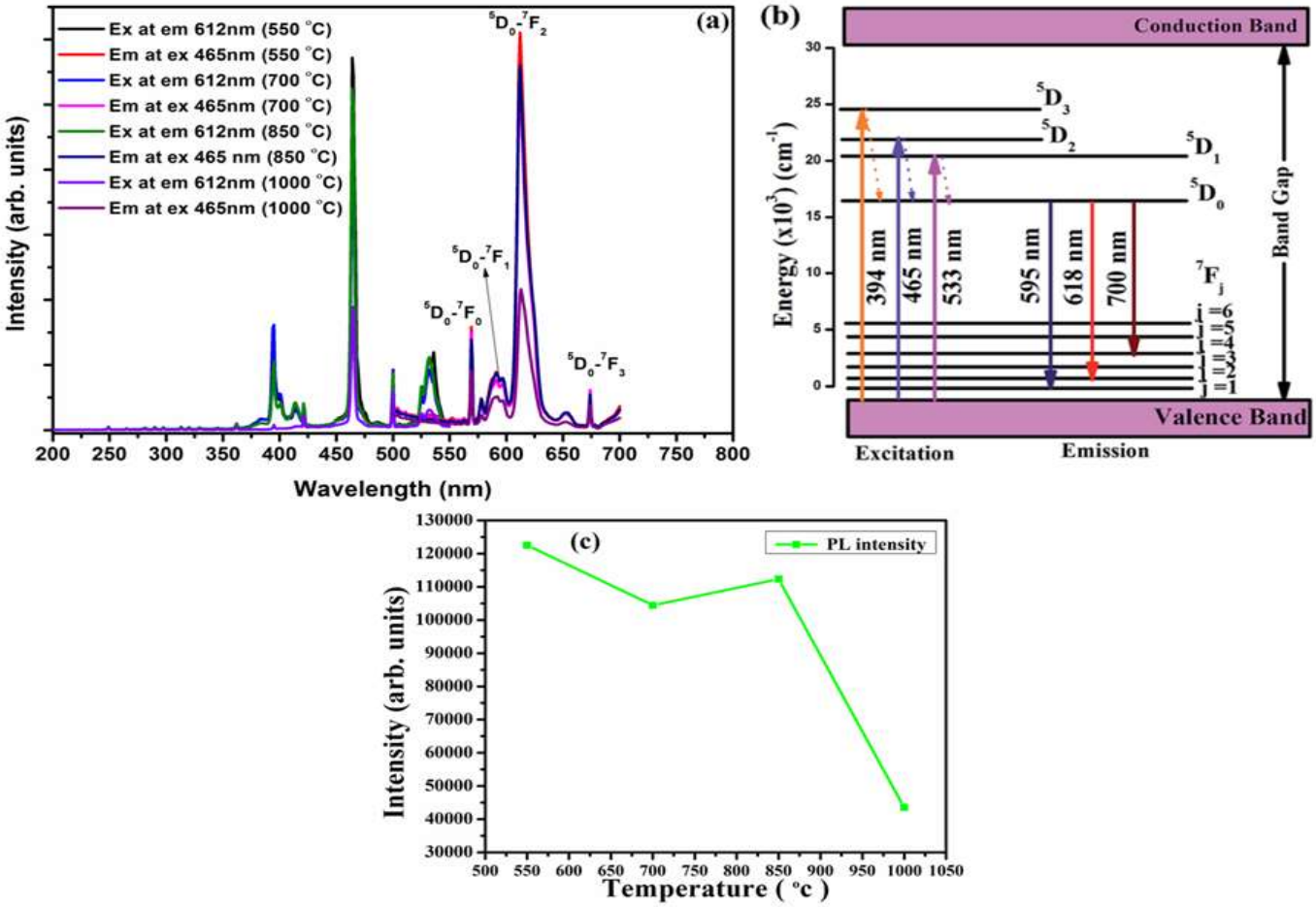

Figure 8: (a) PL spectra of TiO_2 doped with Eu (3 mol%) annealed at different temperatures, (b) energy level diagram of variation of Eu^{3+} and (c) PL intensity of annealed TiO_2:Eu (3 mol%).

Conclusion

A sol–gel method has been applied in order to prepare TiO_2:Eu nanoparticles. When mediated by different structural controlling reagents it produces TiO_2:Eu nanoparticles with different morpho-structural and luminescent properties. The optical properties of the samples were correlated with the structure and composition studied as a function of Eu doping concentration in the TiO_2 host as well as annealing

temperature. The Eu^{3+} doped TiO_2 nanoparticles exhibit red emission peak centered at 612 nm under 465 nm UV light excitation. The luminescence intensity increases with Eu^{3+} concentration up to 3 mol% and then decreases. The decrease of luminescence with increasing Eu^{3+} is related to a self-quenching of the concentration effect. Photoluminescence confirmed that the emission decreased with increasing the annealed temperature.

Acknowledgments

The work was supported by the South African Research Chairs Initiative of the Department of Science and Technology and National Research Foundation of South Africa (grand 84415). The financial assistance of the National Research Foundation (NRF) and the University of the Free State is appreciated. The PL system used is supported by the Rental Pool Programme of the National Laser Centre (NLC).

References

Asahi R, T. Y. (2000). Electronic and optical properties of anatase TiO_2. *Phys Rev B* , 7459-7465.

B. Balasubramanian, K. K. (2010). Synthesis of monodisperse TiO_2-Paraffin core-shell nanoparticles for improved dielectric properties. *ACS Nano* , 1893–1900.

C, L., M, S., O, P., Suciu, C. A., R.C, S., & T.D., G. (2013). Properties of Eu doped TiO_2 nanoparticles prepared by using organic additives. *Journal of Alloys and Compounds* , 29–39.

Choi, W., Termin, A., & Hoffmann, M. R. (1994). Effects of Metal-Ion Dopants on the Photocatalytic Reactivity of Quantum-Sized TiO_2 Particles Angew. *Chem.* , 106, 1148.

Dihingia, P., & Rai, S. (2012). Synthesis of TiO_2 nanoparticles and spectroscopic upconversion luminescence of Nd3+-doped TiO_2–SiO_2 composite glass. . *j. jlumin* , 1243–1251.

Frindell KL, B. M. (2002). Sensitized luminescence of trivalent europium by three-dimensionally arranged anatase nanocrystals in mesostructured titania thin films. *Angew Chem Int Ed* , 959-962.

Javier Navas, A. S.-C.-L.-C. (2014). Thermo-selective TmxTi1−xO2−x/2 nanoparticles: from Tm-doped anatase TiO_2 to a rutile/ pyrochlore $Tm_2Ti_2O_7$ mixture. An experimental and theoretical study with a photocatalytic application. *J Nanoscale* , 12740.

Jiang, K. J., Kitamura, T., Yin, H., Ito, S., & Yanagida, S. (2002). Dye-sensitized Solar Cells Using Brookite Nanoparticle TiO_2 Films as Electrodes. *Chem. Lett.* , 872–873.

Jribi, R. e. (2009). Ultraviolet irradiation suppresses adhesion on TiO_2. *The Journal of Physical Chemistry* , 8273–8277.

Ketteler, G. e. (2007). The nature of water nucleation sites on TiO_2 (110) surfaces revealed by ambient pressure X-ray photoelectron spectroscopy. . *The Journal of Physical Chemistry C* , 8278–8282 .

Koelsch, M., Cassaignon, S., Guillemoles, J. F., & Jolivet, J. P. (2002). Comparison of optical and electrochemical properties of anatase andbrookite TiO_2 synthesized by the sol–gel method. *Thin Solid Film* , 312- 319.

Kumar S, J. Z. (2011). Solvothermally synthesized europium-doped CdS nanorods: applications as phosphors. *J Nanopart Res* , 5465-5471.

Lei Y, Z. L. (2001). Fabrication, characterization and photoluminescence properties of highly ordered TiO_2 nanowire arrays. *J Mater Res* , 1138-1144.

Leostean, C., Stefan, M., Pana, O., Cadis, A., Suciu, R., Silipas, T., et al. (2013). Properties of

Eu doped TiO_2 nanoparticles prepared by using organic additives. *Journal of Alloys and Compounds* , 29–39.

Leshuk, T. e. (2013). Photocatalytic activity of hydrogenated TiO_2. *ACS applied materials & interfaces* , 1892–1895.

Linsebigler, A., Lu, G., & Yates, J. T. (1995). Photocatalysis on TiO_2 Surfaces: Principles, Mechanisms and Selected Results. *Chem. Rev.* , 735- 758.

Liu Y, C. R. (1997). Blue light emitting nanosized TiO_2 colloids. . *J Am Chem Soc* , 5273-5274.

M. H. M. Abdelrehman, V. C. (2020). Effect of background atmosphere and substrate temperature on SrO:Bi3+(0.2 mol%) thin films produced using pulsed laser deposition with different lasers. *Physica B: Condensed Matter* , 411757.

M. Stefan, O. P. (2013). Synthesis and Spectral Characterization of Eu Doped TiO_2 Nanoparticles,. Processes in Isotopes and Molecules . *AIP Conf. Proc* , 259-262.

MASUDA, & Akimasa. (2001). A more comprehensive interpretation of distinct discontinuity in rare-earth element dissolution by HCl-HNO_3 from silicate rock powder. *Proceedings of the Japan Academy. Ser. B: Physical and Biological Sciences* , 187- 190.

McHale, e. L. (2012). *Handbook of luminescent semiconductor materials.* Boca Raton: CRC Press.

Ogawa, H., Higuchi, T., Nakamura, A., Tokita, S., Miyazaki, D., Hattori, T., et al. (2008). Growth of Sc-Doped TiO_2 Thin Film by RF Magnetron Sputtering. *Japanese Journal of Applied Physics, Alloys Compd* , 375.

Pal, M., Pal, U., Jiménez, J. M., & Pérez-Rodríguez, F. (2012). Effects of crystallization and dopant concentration on the emission behavior of TiO_2: Eu nanophosphors. *J Nanoscale research letters* , 1-12.

R. Nainani, P. T. (52-58.). Synthesis of Silver Doped TiO_2 Nanoparticles for the Improved Photocatalytic Degradation of Methyl Orange. *J. Mater. Sci. Eng* , 2012.

Reddy, K. M., Manorama, S. V., & Reddy, A. R. (2003). Bandgap studies on anatase titanium dioxide nanoparticles. *Mater. Chem. Phys.* , 239–245.

S. Yao, L. X. (2011). Properties of Eu3+ luminescence in the monoclinic Ba2MgSi2O7. *Ceramics* , 251-255.

Sharma, S. S. (2012). Eu3+/Tb3+ co-doped Y_2O_3 nanophosphors: Rietveld refinement, bandgap and photoluminescence optimization. *J. Phys. D Appl. Phys.* , 415102.

Sharmy Saimon Mano, K. K. (2012,). Effect of Polyethylene Glycol Modification of TiO_2 Nanoparticles on Cytotoxicity and Gene Expressions in Human Cell Lines. *J. Mol. Sci.* , 3703-3717.

Sibu, C. P., Kumar, S. R., Mukundan, P., & Warrier, K. G. (2002). Titania nanostructured coating for corrosion mitigation of stainless steel Chem. . *Mater., 2002, 14, 2876* , 14, 2876.

Simmons, E. (1974). *The application of diffuse reflectance spectroscopy to the chemistry of transition metal coordination compounds.*

Simonsen, M. E. (2009). Influence of the OH groups on the photocatalytic activity and photoinduced hydrophilicity of microwave assisted sol–gel TiO_2 film. *Applied Surface Science* , 8054–8062.

Stefanov, P. e. (012039). XPS characterization of TiO_2 layers deposited on quartz plates. *Journal of Physics: Conference Series 100* , 2008.

Su, Y., Lang, J., Li, L., Guan, K., Du, C., Peng, L., et al. (2013). Unexpected Catalytic

Performance in Silent Tantalum Oxide through Nitridation and Defect Chemistry. *J.American Chemical Society* , 11433–11436.

T. Lo´ pez, J. H.-V. (2001). *J. Mol. Catal. A: Chem.* , 2001.

Tang, H., Prasad, K., Sanjines, R., Schmid, P. E., & Levy, F. (1994). Electrical and optical properties of TiO_2 anatase thin films. *Appl. Phys.* , 2042–2047.

Tiwana, P., Docampo, P., Johnston, M., Snaith, H., & Herz, L. (2011). Electron Mobility and Injection Dynamics in Mesoporous ZnO, SnO_2, and TiO_2 Films Used in Dye-Sensitized Solar Cells. *ACS Nano* , 5 (6) 5158–5166.

Toma, F., Bertrand, G., Begin, S., Meunier, C., Barres, O., Klein, D., et al. (2006). advanced Ceramic Coatings and Materials for Extrem Environments Appl. *Catal* , 74.

W. Li, C. N., Lin, H., Huang, C. P., & Shah, S. I. (2004). Size Dependence of Thermal Stability of TiO_2 Nanoparticles. *J. Appl. Phys.* , 6663–6668.

Wang, Y. e. (2013). Role of point defects on the reactivity of reconstructed anatase titanium dioxide (001) surface. *Nature communications* , 1038.

Yu J, X. Q. (2009). Preparation, characterization and visible-lightdriven photocatalytic activity of Fe-doped titania nanorods and firstprinciples study for electronic structures. *Appl Catalysis B: Environmetal* , 595-602.

Yuhong, Z., Huaxing, Z., X.Yongxi, & Yanguang, W. (2003). Europium doped nanocrystalline titanium dioxide: preparation, phase transformation and photocatalytic properties. *Journal of Materials Chemistry* , 2261.

Yuta Tanaka1, H. S. (2008). , Active Hydroxyl Groups on Surface Oxide Film of Titanium, 316L Stainless Steel, and Cobalt-Chromium-Molybdenum Alloy and Its Effect on the Immobilization of Poly(Ethylene Glycol). *Materials Transactions* , 805 - 811.

Z, X., Q, Y., & al., X. C. (2005). Structure, luminescence properties and photocatalytic activity of europium doped-TiO_2 nanoparticles. *J Mater Sci* , 1539–1541 .

Z. Sarteep, A. E. (2016). Silver Doped TiO_2 Nanoparticles: Preparation, Characterization and Efficient Degradation of 2,4-dichlorophenol Under Visible Light. *J. Water Environ. Nanotechnol* , 135-144.

Zhang WF, Z. M. (2000). Microstructures and visible photoluminescence of TiO_2 nanocrystals. *Phys Stat Sol* , 319-327.